Nutrient Replenishment by Turbulent Mixing in Suspended Macroalgal Farms

Tong Bo[1], James C. McWilliams[1], Christina A. Frieder[2], Kristen A. Davis[3,4], Marcelo Chamecki[1]

[1]Department of Atmospheric and Oceanic Sciences, University of California, Los Angeles, Los Angeles, CA, USA
[2]Southern California Coastal Water Research Project, Costa Mesa, CA, USA
[3]Department of Civil and Environmental Engineering, University of California, Irvine, Irvine, CA, USA
[4]Department of Earth System Science, University of California, Irvine, Irvine, CA, United States

Key Points:

- Suspended macroalgal farms can enhance turbulence and drive upward nutrient fluxes from below the farm base to prevent starvation.
- The Damkohler number, comparing nutrient transport with uptake by macroalgae, can be used to predict nutrient availability in the farm.
- Farming strategies are proposed such as timely harvesting and selecting locations with a shallow nutricline and robust currents and waves.

Corresponding author: Tong Bo, tbo@atmos.ucla.edu

Abstract

This study uses large eddy simulations to investigate nutrient transport and uptake in suspended macroalgal farms. Various farm configurations and oceanic forcing conditions are examined, with the farm base located near the nutricline depth. We introduce the Damkohler number Da to quantify the balance between nutrient consumption by macroalgae uptake and supply by farm-enhanced nutrient transport. Most cases exhibit $Da < 1$, indicating that farm-generated turbulence sufficiently contributes to upward nutrient fluxes, supporting macroalgae growth. High Da and starvation may occur in fully grown farm blocks, a configuration that generates weakest turbulence, particularly when combined with densely planted macroalgae or under weak flow conditions. Flow stagnation within the farm due to macroalgae drag may constrain the uptake efficiency and further increase the starvation risk. Mitigation strategies involve timely harvesting, avoiding dense macroalgae canopies, and selecting farm locations with robust ocean currents and waves. This study provides insights for sustainable macroalgal farm planning.

Plain Language Summary

Offshore macroalgal farming has been proposed as a sustainable strategy for carbon sequestration, biofuel production, food supply, and bioremediation. However, challenges arise as macroalgal farms are typically suspended above the nutricline and may thus deplete the existing nutrient inventory near the sea surface. In this study, large eddy simulations reveal that suspended farms can generate intense turbulence and drive upward nutrient fluxes from below the farm base. Various farm simulations are conducted, and in most cases the farm-generated turbulence is indicated to provide sufficient nutrient fluxes to support macroalgae growth. This presents a self-sustaining solution for nutrient supply through passive entrainment. To mitigate the risk of farm starvation, we propose strategies such as timely harvesting, avoiding dense macroalgae canopies, and selecting farm locations with robust ocean currents and waves.

1 Introduction

Marine macroalgae play a vital role in maintaining ecosystem health by serving as crucial habitats and providing food sources for a diverse range of marine species (e.g., Dayton, 1985; Teagle et al., 2017). Beyond their ecological importance, the cultivation of macroalgae has been proposed as a sustainable strategy for carbon sequestration, biofuel production, food supply, and bioremediation (Ghadiryanfar et al., 2016; Ferdouse et al., 2018; Arzeno-Soltero et al., 2023). Recent interest has grown in expanding macroalgal farming offshore utilizing suspended structures, due to difficulty of permitting and competing uses for shallow, nearshore coastal regions (Troell et al., 2009; Fernand et al., 2017; Frieder et al., 2022; Arzeno-Soltero et al., 2023).

The suspended macroalgal farms are typically located within the upper mixed layer of the ocean. A crucial factor affecting farm performance is the interaction of suspended farms with hydrodynamic processes in the mixed layer (Yan et al., 2021; Frieder et al., 2022). Macroalgae exert drag force on the flow, causing current and wave attenuation (Thom, 1971; Jackson, 1997; Rosman et al., 2007; Monismith et al., 2022). Discontinuities in drag can lead to the development of shear layers and eddies at the edges of the farm (Plew, 2011; Yan et al., 2021). In addition, enhanced Langmuir-type circulations can be created within farms due to the interplay between surface gravity waves and farm-modulated currents (Yan et al., 2021; Bo et al., 2024). Moreover, these farm-generated hydrodynamic processes also exhibit a distinct dependence on farm configurations (Poggi et al., 2004; Bailey & Stoll, 2013; Bo et al., 2024). The varied hydrodynamic responses associated with different farm configurations can consequently result in various impacts on the mixing and transport of chemicals and nutrients.

Optimal farm design ensures an adequate nutrient supply for cultivated macroalgae throughout the canopy. Challenges arise as suspended farms are usually positioned near the sea surface where nutrient concentrations are relatively low (Frieder et al., 2022; Arzeno-Soltero et al., 2023). Farm starvation may occur due to either a complete absence of background nutrients in the mixed

layer caused by larger scale ocean dynamics and biogeochemistry, where the concentration is below the criteria for farm growth, or when there is initially sufficient background nutrient, but rapid macroalgal consumption depletes the existing nutrient inventory within the farm. Turbulence and coherent eddies generated by these farms have the potential to induce significant vertical mixing (Nepf et al., 2007; Abdolahpour et al., 2017; Yan et al., 2021), leading to the consistent entrainment of nutrients from below the farm base to prevent starvation. This introduces a self-sustaining mechanism for passive nutrient supply to the farm (Frieder et al., 2022). Considering the variability of farm-generated turbulence associated with distinct farm configurations (Yan et al., 2021; Bo et al., 2024), further investigation into nutrient transport and uptake by the farm is therefore essential for optimally designing farm layouts to ensure nutrient availability and support macroalgae growth.

This study uses large eddy simulations (LES) to investigate nutrient transport and uptake associated with suspended macroalgal farms, aiming to understand the hydrodynamic aspects influencing nutrient availability for farm growth. Section 2 describes the numerical approach and the various farm simulations examined in this study. In section 3, we analyze farm-generated turbulence and nutrient fluxes across different simulation settings. We also investigate nutrient uptake associated with varied farm configurations, and compare the relative impacts of nutrient uptake versus turbulent transport in determining nutrient availability. Section 4 discusses potential factors affecting farm performance and concludes the study.

2 Methods

2.1 LES model description

The LES method is used to study the hydrodynamics, nutrient transport, and uptake associated with the macroalgae of interest, here parameterized for giant kelp, *Macrocystis pyrifera*. We choose LES as it can effectively capture the intricate mixing processes driven by farm-generated turbulence. The LES framework is based on a set of wave-averaged and grid-filtered equations for velocity, temperature, and passive tracer (see Supporting Information Text S1 for details). Specifically, the Craik–Leibovich vortex force and Coriolis force are included to represent the influences of surface gravity waves and planetary rotation (Craik & Leibovich, 1976; McWilliams et al., 1997). The code has been validated and used in previous macroalgal farm and boundary layer flow studies (Yan et al., 2021, 2022; Bo et al., 2024).

The resistance imposed by kelp onto the flow is parameterized as a drag force F_D in the momentum equation, and is expressed as

$$\boldsymbol{F}_D = \frac{1}{2} C_D a \boldsymbol{P} \cdot (|\boldsymbol{u}|\boldsymbol{u}) \,. \tag{1}$$

The velocity vector $\boldsymbol{u} = (u, v, w)$, including the streamwise (x), cross-stream (y), and vertical (z) components, respectively. Here, $C_D = 0.0148$ is the drag coefficient according to the experimental study of Utter & Denny (1996) and numerical validation in Yan et al. (2021), and a is the frond surface area density (area per volume, m^{-1}) obtained by conversion of the algal biomass (Frieder et al., 2022). The coefficient tensor $\boldsymbol{P}$ stands for the projection of frond surface area into each direction, and in the present study we use $\boldsymbol{P} = (1/2)\boldsymbol{I}$, where $\boldsymbol{I}$ is the identity matrix (Yan et al., 2021).

Nutrients are treated as a passive tracer in the model, and in specific we focus on nitrate in this study as it is the limiting macronutrient in many coastal regions where *Macrocystis pyrifera* grows. Nutrient uptake by kelp is treated as a sink term $\mathcal{S}$ in the tracer transport equation, written as

$$\mathcal{S} = a V_{max} \frac{N}{N + K_M}. \tag{2}$$

This is the Michaelis-Menten formula (Michaelis et al., 1913; Cornish-Bowden, 2015), where the uptake rate saturates and approaches the maximum value V_{max} as nitrate concentration N increases. Here $K_M = 10.2$ μM (micromolar) is the half saturation constant of nitrate for *Macrocystis pyrifera*,

and $V_{max} = 0.2$ μmol m^{-2}s^{-1} is used as a representative value (Gerard, 1982; Haines & Wheeler, 1978; Frieder et al., 2022; Arzeno-Soltero et al., 2023). Besides, a couple of simulations are conducted with V_{max} increased by a factor of three to investigate an end-member scenario with a high uptake rate (Arzeno-Soltero et al., 2023).

In addition, the dependence of uptake on flow speed is examined by adding a velocity factor $\mathcal{F}(|\boldsymbol{u}|)$ to the Michaelis-Menten formula (Broch & Slagstad, 2012), i.e.,

$$\mathcal{S} = aV_{max}\frac{N}{N+K_M}\mathcal{F}(|\boldsymbol{u}|) = aV_{max}\frac{N}{N+K_M}\left[1-\exp\left(-\frac{|\boldsymbol{u}|}{u_{ref}}\right)\right]. \tag{3}$$

The rationale behind this velocity factor is that, at low velocities, the thick diffusive boundary layers surrounding kelp fronds pose constraints on the nutrient uptake rate (Stevens & Hurd, 1997; Huang et al., 2011). In contrast, at higher velocities the boundary layer thickness is no longer a limiting factor, and Equation (3) approaches the Michaelis-Menten formula in Equation (2). The reference velocity $u_{ref} = 0.03$ m s^{-1} (Stevens & Hurd, 1997; Broch & Slagstad, 2012) corresponds to the velocity at which the uptake reaches 65% of the optimal rate. Using more intricate formulas could introduce additional variability in the uptake rate, e.g., those explicitly incorporating the boundary layer thickness and the periodic perturbations by waves (Stevens & Hurd, 1997; Huang et al., 2011; Frieder et al., 2022), but here for simplicity we use this empirical velocity dependence formula by Stevens & Hurd (1997) and Broch & Slagstad (2012).

2.2 Farm simulation setup

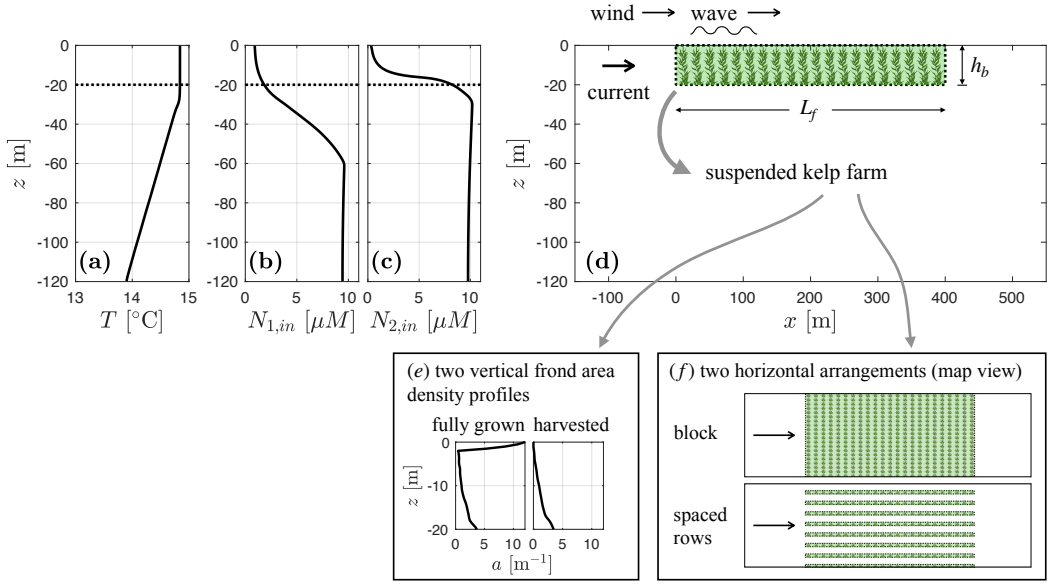

Figure 1. Simulation setup. (a): Temperature profile at the upstream boundary (inflow condition). (b) and (c): Two inflow nutrient profiles. Dotted black lines indicate the farm base. (d): A schematic of the farm simulation (side view), with vertical profiles of frond area density (e) and map views of farm configurations (f) in the auxiliary subfigures.

The cultivation of macroalgae in open ocean environments involves a diverse range of aquaculture structures. A representative farm configuration considered here consists of a series of organized longlines spaced horizontally (Yan et al., 2021; Frieder et al., 2022). Each longline is deployed at a constant depth, anchored at both ends and also connected to surface buoys. *Macrocystis pyrifera*

is cultivated along growth ropes attached to the longlines, and will grow upright toward the surface due to their buoyancy.

Macroalgal farm simulations are conducted on a $800 \times 208 \times 120$ m^3 domain, with $400 \times 104 \times 240$ uniformly distributed grid cells. A turbulent flow undisturbed by the presence of the farm is input from the upstream boundary, and the analyses focus on a period during which the background flow has fully adapted to the presence of the suspended farm (details provided in Supporting Information). The farm is located in the middle of the domain from $x = 0$ to $x = L_f$, with a farm length of $L_f = 400$ m (Figure $1(d)$). The upstream boundary is at $x = -150$ m, and the downstream boundary is at a distance of 250 m from the farm trailing edge. In the y-direction the farm extends across the entire domain with a periodic boundary, i.e., effectively assuming an infinite farm width. In the vertical direction the farm is between the sea surface and $h_b = -20$ m (the farm base), i.e., the depth at which the suspended longlines are deployed.

Two types of horizontal farm arrangements are examined (Figure $1(f)$). The first type has the spaced longlines (farm rows) aligned parallel to the x-direction, extending the length of the farm. The second type assumes a scenario where the kelp rows are deployed closely enough so that there is no gap in between, i.e., essentially forming a horizontally uniform kelp farm block. In addition, two vertical profiles of frond surface area density a are considered (Figure $1(e)$), representing two different growth stages of kelp (Frieder et al., 2022): (1) a fully grown profile, where kelp extends from the farm base to the sea surface, with notably high frond area density at the top due to a large portion of the fronds floating at the sea surface; (2) a harvested profile, where the frond density is reduced to zero in the uppermost 1-2 m part of the farm near the sea surface, as a result of harvest practices. The frond surface area density profiles of the two stages are obtained by conversion of the algal biomass (Frieder et al., 2022), with depth-averaged values of 2 and 1 m^{-1}, respectively. Additionally, each profile is multiplied by a factor of 0.3 or 3, to investigate the influence of decreased or increased kelp density.

The external forcing conditions are generally the same as those in McWilliams et al. (1997), Yan et al. (2021), and Bo et al. (2024). A geostrophic current $u_g = 0.2$ m s^{-1} is imposed in x-direction, representing the effect of mesoscale flow. The Coriolis frequency $f = 10^{-4}$ s^{-1} corresponds to around 45° N latitude. A constant wind stress $\tau_w = 0.037$ N m^{-2} is applied at the surface boundary, corresponding to a wind speed at 10-m height above the surface of 5 m s^{-1}. The surface gravity waves have an amplitude of $A_w = 0.80$ m, and the wavelength $\lambda_w = 60$ m. In addition, we explore another set of weaker current, wind, and wave conditions to investigate variability in external forcing, where $u_g = 0.05$ m s^{-1}, $\tau_w = 0.009$ N m^{-2}, and $A_w = 0.57$ m.

The initial mixed layer depth at the upstream boundary (inflow) is 25 m (Figure 1 (a)), and a stably stratified layer is beneath it, with a uniform temperature gradient $\mathrm{d}\theta/\mathrm{d}z = 0.01$ K m^{-1}. We assume no heat flux at the surface boundary. Two background (inflow) nutrient profiles are examined in this study. The first profile (N_1) is obtained from the representative nutrient condition of the realistic California Current System model (Deutsch et al., 2021; Renault et al., 2021; Frieder et al., 2022), featuring a relatively weak vertical gradient within the mixed layer, a strong gradient below the mixed layer (considered as a nutricline), and a uniformly high concentration of around 10 μM below 60m (Figure 1 (b)). The second profile (N_2) exhibits a relatively strong vertical gradient within the mixed layer and a uniform concentration of 10 μM below the mixed layer (Figure 1 (c)), representing a scenario with a shallower nutricline.

More detailed descriptions of simulation setup and farm configurations are provided in Supporting Information. Note that this study does not delve into the intricate mechanisms of how various farm configurations and forcing conditions lead to distinct hydrodynamic conditions and nutrient mixing; these aspects were addressed in a prior study by Bo et al. (2024). Instead, our major objective in conducting a range of farm simulations is to generate variable levels of nutrient mixing and uptake and to examine how their balance influences nutrient availability within the farm.

3 Results

In this section we present the hydrodynamics, nutrient transport, and uptake associated with the kelp farm. We first introduce a flow decomposition to separate distinct transport processes. The instantaneous flow field can be split into the mean flow, standing eddies, and turbulence, i.e.,

$$\boldsymbol{u} = \langle \overline{\boldsymbol{u}} \rangle_y + \overline{\boldsymbol{u}}^s + \boldsymbol{u}'. \tag{4}$$

The overline represents the time average, and the prime represents temporal fluctuations around the time average, i.e., the turbulent component. Here $\langle \cdot \rangle_y$ denotes the cross-stream average, and the superscript "s" denotes the standing-eddy component (time-averaged spatial variations in y-direction generated by the farm structure). Similarly, the covariance between velocity and nutrient concentration can be decomposed as

$$\left\langle \overline{\boldsymbol{u}N} \right\rangle_y = \langle \overline{\boldsymbol{u}} \rangle_y \left\langle \overline{N} \right\rangle_y + \left\langle \overline{\boldsymbol{u}}^s \overline{N}^s \right\rangle_y + \left\langle \overline{\boldsymbol{u}'N'} \right\rangle_y . \tag{5}$$

The second term on the right side stands for the cross-stream-averaged nutrient transport driven by the standing eddy, effectively a dispersive flux (Finnigan, 2000), and the third term represents the turbulent flux.

3.1 Farm-enhanced boundary layer eddies

As ocean currents enter the farm, the mean flow is decelerated due to the drag force exerted by the kelp. The kelp drag discontinuity at the farm bottom edge enhances the vertical shear of streamwise velocity, leading to the development of shear layer eddies (Figure $2(a)$). Here we specifically consider the vertical component w' when discussing turbulence intensity, because of its direct relevance to vertical transport in kelp farms. Moreover, Langmuir-type turbulence is generated within the farm due to the combined effects of waves and farm-modulated currents (Yan et al., 2021; Bo et al., 2024). The farm-generated Langmuir turbulence exhibits a stronger magnitude compared to the standard Langmuir turbulence in the upstream region, which typically occurs in the surface boundary layer without the presence of kelp (McWilliams et al., 1997). In addition to turbulence, standing eddies occur exclusively in farm configurations with horizontally spaced kelp rows (Yan et al., 2021; Bo et al., 2024) (Figure $2(b)$). The strength of the farm-generated turbulence and standing eddies varies with farm configurations and oceanic forcing conditions (Bo et al., 2024), and these variations thus lead to different vertical transport of nutrients, as detailed in the subsequent section.

3.2 Vertical nutrient fluxes

Both farm-generated turbulence and standing eddies can drive upward nutrient fluxes (Figure $2(c)$ and (d)). To quantify the strength of farm-generated vertical mixing, we define the turbulent and standing-eddy mixing coefficients (κ_t and κ_s) based on the cross-stream-averaged fluxes in Equation (5),

$$\kappa_t = \frac{\left\langle \overline{w'N'} \right\rangle_y}{\mathrm{d}\left\langle \overline{N} \right\rangle_y / \mathrm{d}z}, \tag{6a}$$

$$\kappa_s = \frac{\left\langle \overline{w}^s \overline{N}^s \right\rangle_y}{\mathrm{d}\left\langle \overline{N} \right\rangle_y / \mathrm{d}z}. \tag{6b}$$

The mixing coefficients calculated with the two nutrient profiles N_1 and N_2 are generally consistent, and we use profile N_2 for the calculation of mixing coefficients, because its stronger vertical gradients on the denominator provide more robust results.

More in-depth analyses of how various farm configurations lead to distinct turbulence intensities have been conducted by (Bo et al., 2024), and we provide a concise summary here. In spaced kelp rows aligned with the background current, both turbulence and standing eddies occur irre-

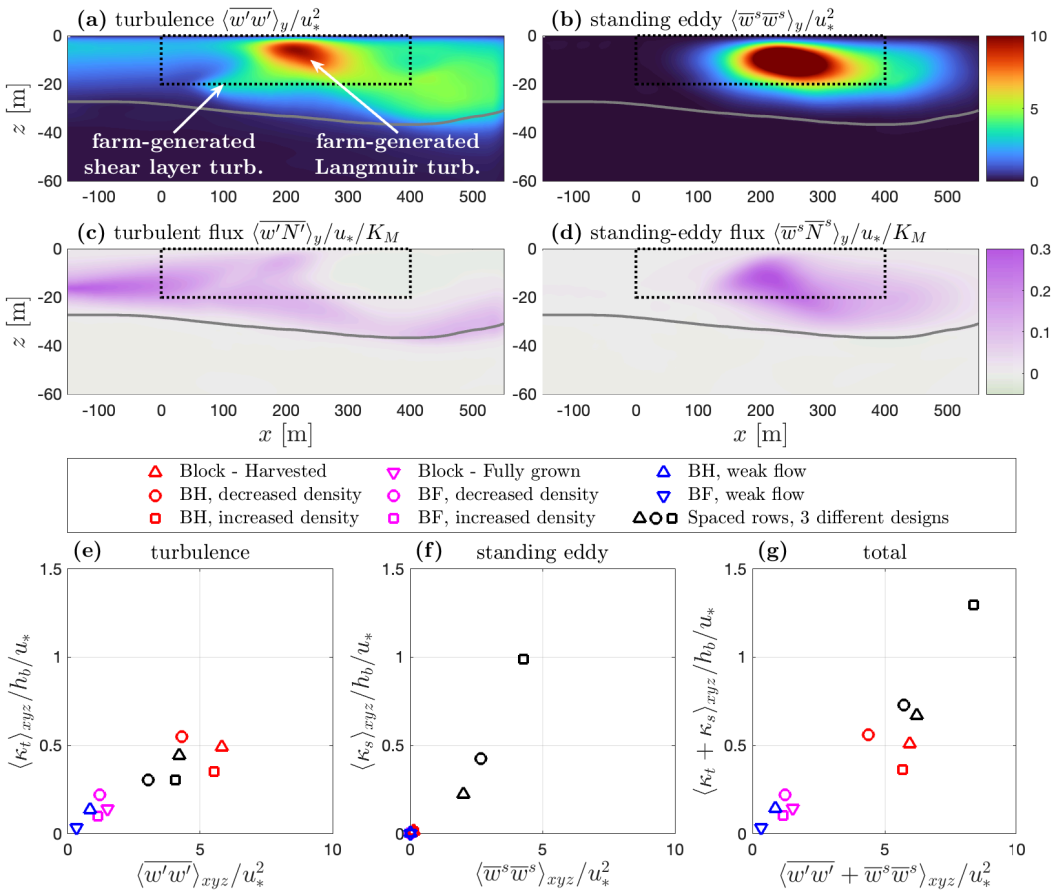

Figure 2. Eddies and nutrient fluxes associated with the kelp farm, in a simulation with horizontally spaced kelp rows. (a) and (b): Side views of turbulence and standing eddy intensity (the vertical component). Dotted rectangles show the extent of the farm, and the solid gray lines represent the mixed layer depth. (c) and (d): Side views of vertical nutrient fluxes driven by turbulence and standing eddies for profile N_2. (e) – (g): Turbulent (e), standing-eddy (f), and total (g) mixing coefficients versus turbulence or eddy intensity (averaged within the farm) for various simulations. The detailed parameters for different simulations can be found in Table S1 in Supporting Information.

spective of the vertical kelp frond density distribution, leading to the corresponding nutrient fluxes (Figure 2(e) and (f)). In contrast, standing eddies do not occur in farm blocks. Relatively strong turbulence and nutrient mixing are found in farm blocks with a harvested profile, while turbulent mixing is weak in cases with a fully grown profile due to an inhibition mechanism of Langmuir circulation by this frond distribution (Bo et al., 2024). Additionally, turbulence intensity and mixing decrease in simulations with weaker currents and waves.

The mixing coefficients generally exhibit a positive correlation with the corresponding turbulence (or eddy) intensity across various simulations (Figure 2(e), (f), and (g)). This is in agreement with the mixing length theory, where the mixing coefficient scales with the eddy-velocity-scale multiplied by a length-scale. The mixing length for turbulence appears to be much smaller than the farm height (approximately $0.2h_b$), consistent with findings by Abdolahpour et al. (2017). The standing-eddy mixing coefficient has a steeper slope dependence on its corresponding eddy intensity than the turbulent mixing coefficient, indicating that the standing eddies responsible for driving nutrient fluxes have a larger size (up to $0.5h_b$) compared to turbulence.

3.3 Nutrient supply versus uptake

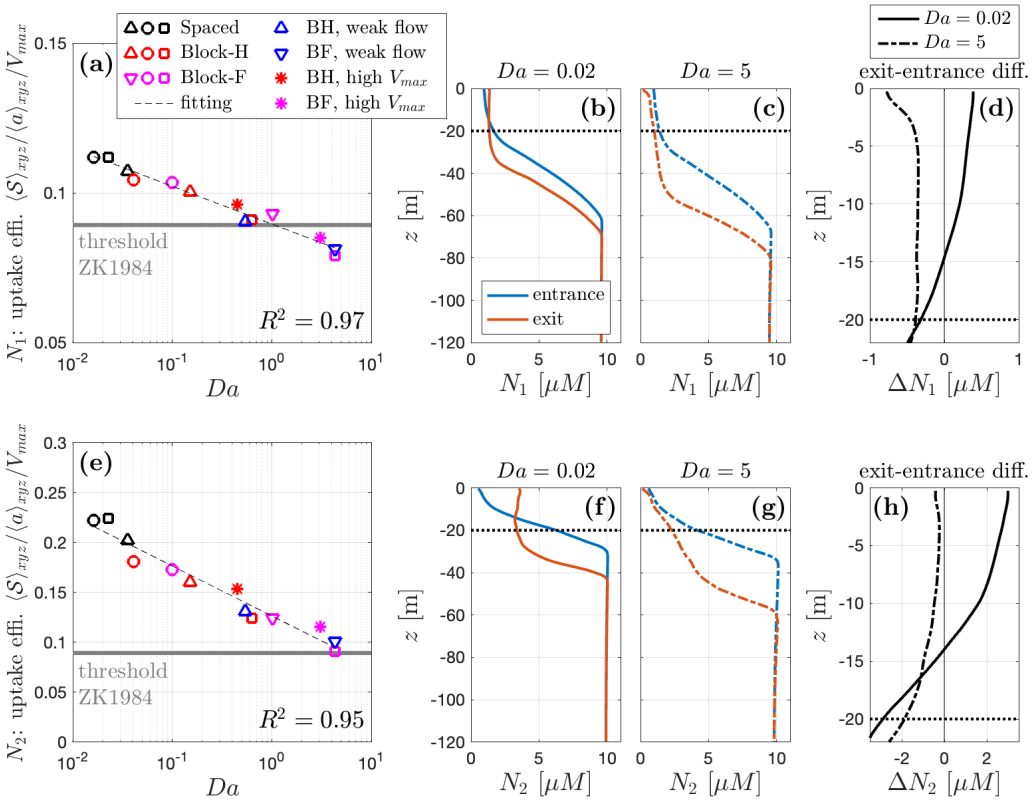

Figure 3. Dependence of farm nutrient availability on Da. (a): Uptake efficiency versus Da across different simulations, for nutrient profile N_1 (Figure $1(b)$). Case symbols are consistent with Figure 2. The horizontal gray line is the estimated threshold for kelp growth according to Zimmerman & Kremer (1984). (b) and (c): Vertical nutrient profiles at the farm entrance and exit, for simulations with a low and high Da ($Da = 0.02$ and $Da = 5$), respectively. (d): Exit-entrance difference for low and high Da. $(e) - (h)$: A similar set of plots for nutrient profile N_2 (Figure $1(c)$).

While farm-generated turbulence can lead to upward fluxes that increase nutrient availability in the farm, kelp uptake consumes nutrients and may thus result in nutrient depletion and kelp starvation. In this section, we consider the Michaelis-Menten uptake equation (2) and compare the influence of nutrient uptake to farm-generated nutrient fluxes. We define a farm-averaged Damkohler number (e.g., Rehage & Kind, 2021)

$$Da = \frac{\tau_{mix}}{\tau_{uptake}} = \frac{\langle a \rangle_{xyz} V_{max} h_b^2}{\langle \kappa_t + \kappa_s \rangle_{xyz} K_M}, \tag{7}$$

which compares the mixing timescale $\tau_{mix} = h_b^2 / \langle \kappa_t + \kappa_s \rangle_{xyz}$ with the uptake timescale $\tau_{uptake} = K_M / (\langle a \rangle_{xyz} V_{max})$ from Equation (2). Note that both the frond area density a and turbulent and standing-eddy mixing coefficients κ_t and κ_s vary with farm configurations. Da effectively quantifies the relative strength of nutrient consumption by uptake versus vertical mixing that supplies nutrient, with $Da \ll 1$ indicating strong mixing, and vice versa.

The Damkohler number Da demonstrates a clear correlation with nutrient availability in the farm, quantified here as a dimensionless uptake efficiency $\mathcal{S}/a/V_{max}$ (Figure 3(a)). For low Da, nutrient entrainment from below the farm exceeds the uptake rate, ensuring adequate nutrients for

kelp growth. In this scenario, nutrient concentration is increased at the farm exit compared to the background nutrient profile entering the farm (Figure 3(b) and (d)). In contrast, for high Da, farm-generated nutrient fluxes are insufficient to balance uptake, resulting in nutrient depletion at the farm exit (Figure 3 (c) and (d)) and potentially leading to the threat of starvation. The transition to starvation, estimated by applying the threshold of 1 μM nitrate (Zimmerman & Kremer, 1984) to the Michaelis-Menten formula, occurs at around $Da = 1$ (Figure 3 (a)).

The above analysis is based on the first nutrient profile (N_1, from the realistic California Current System model). The dependence of uptake efficiency on Da also holds for the other nutrient profile (N_2, with stronger vertical gradients near the sea surface, Figure 3 (e)-(h)), except that the variability in uptake efficiency is much greater than that for N_1, because of its greater range of nutrient concentration within the surface boundary layer. The transition to starvation occurs at a larger Da (around 5) for profile N_2.

Overall for nutrient profiles N_1 and N_2, most cases exhibit a small Da, e.g., less than 1, suggesting that farm-generated fluxes can provide adequate nutrients to prevent starvation. Nutrient depletion and high Da are most likely to occur in farm blocks with a fully grown profile, i.e., the farm configuration with the least turbulence generation, in particular when this configuration is combined with dense kelp that increases the uptake rate or weak current and wave conditions that decreases vertical nutrient mixing. Note that the farm blocks typically have a larger farm-averaged frond density $\langle a \rangle_{xyz}$ than spaced rows. However, the increase in Da for farm blocks is beyond that predicted by the increase in a alone, indicating that weakened vertical mixing due to the farm configuration is also a significant contributor to starvation. While in most cases the high uptake rate is attributed to the increased a, two additional simulations with an increased V_{max} also lead to a high uptake rate and reduced nutrient availability, similar to the effect of the increased a.

Additional analysis is included in Supporting Information (Text S2) on how the correlation between uptake efficiency and Da varies with background nutrient profiles. Overall Da proves to be an effective metric for predicting nutrient uptake and farm growth. It is also worth noting that other scenarios for starvation may occur, such as when the nutricline is substantially below the farm base, with a complete absence of nutrients in the mixed layer. This starvation regime is not the focus of the present study, as the farm-generated turbulence would be incapable of transporting nutrients from the deep nutricline.

3.4 Dependence of uptake on hydrodynamic conditions

In addition to the above mentioned factors that may lead to kelp starvation, another critical aspect is the dependency of kelp uptake rate on hydrodynamic conditions. In this section, we investigate the modified Michaelis-Menten uptake formula that integrates the influence of velocity (Equation (3)). The drag exerted by kelp tends to decelerate the mean current within the farm, and this deceleration is particularly pronounced in dense farms (Figure 4(a)). The decreased velocity results in thicker diffusive boundary layers around kelp fronds, resulting in an additional constraint on kelp nutrient uptake (Stevens & Hurd, 1997).

The reduction in uptake rate due to velocity constraints is most notable in cases with weak background ocean currents or high kelp density, both of which can decrease the mean velocity in the farm to less than $\sim$ 0.05 m s^{-1}. The velocity constraint factor in Equation (3) can thus be decreased to approximately 0.7 (Figure 4(b)), leading to a decrease of up to 30% in uptake efficiency (Figure 4 (c)). Moreover, these cases characterized by strong velocity constraints coincide with high Da values as investigated in the previous section. Consequently, the velocity constraint further increases the risk of starvation posed by the low nutrient availability. The uptake efficiency converges toward that obtained by the standard Michaelis-Menten formula in other cases where velocity remains higher than ~ 0.05 m s^{-1} within the farm.

Additionally, the relative reduction in uptake efficiency generally aligns with the velocity-dependence factor calculated from the bulk average streamwise velocity (Figure 4(d)). This suggests that the spatial and temporal variability of velocity within the farm has minimal influences on the

overall uptake, and using the farm-averaged mean velocity is sufficient for predicting the reduced uptake due to velocity constraints.

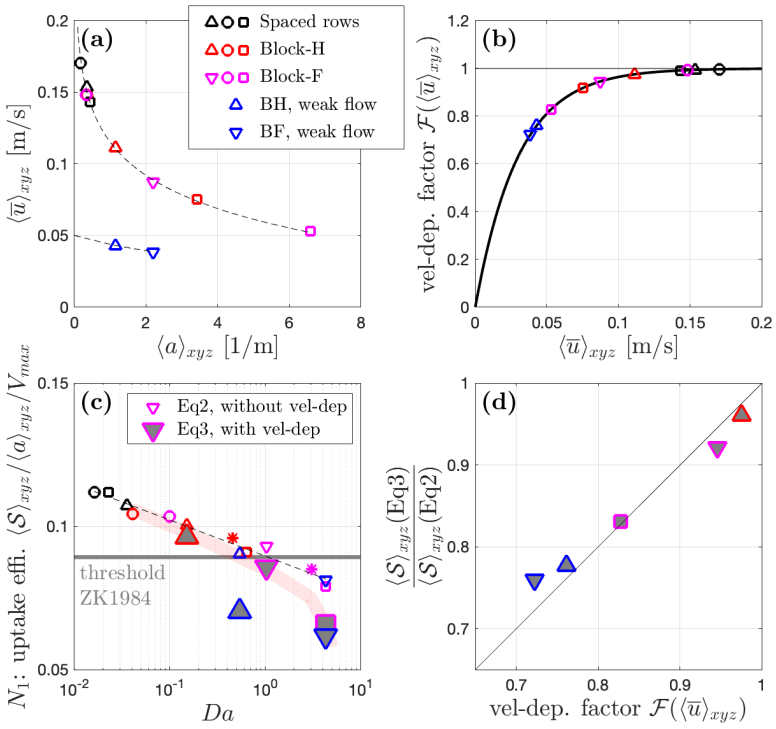

Figure 4. Influences of hydrodynamic conditions on nutrient uptake. (a): Average streamwise velocity within the farm versus average kelp frond area density. Case symbols are consistent with Figures 2 and 3. (b): The velocity dependence factor in Equation (3) as a function of mean flow speed. (c): Uptake efficiency versus Da for nutrient profile N_1. Gray-filled markers represents simulations that incorporate the velocity-dependence of uptake rate based on Equation (3), and the other simulations based on Equation (2) do not have this velocity-dependence. (d): The decrease in uptake efficiency due to velocity constraints (ratio of uptake efficiency, with versus without velocity-dependence in subfigure (c)), compared with the velocity-dependence factor from subfigure (b). Only profile N_1 is shown as an example here, and profile N_2 yields consistent results.

4 Discussion and conclusion

This study investigates the impacts of vertical nutrient fluxes and kelp uptake on nutrient availability in the farm, and the Damkohler number Da is introduced to quantify the competing effects of the two processes. Most investigated farm configurations exhibit a small Da, indicating that farm-generated turbulence can provide sufficient nutrient supply to exceed kelp uptake. This supports the concept of a self-sustaining solution for nutrient supply to the farm through passive entrainment. It is noteworthy that Langmuir-type turbulence mostly prevails over shear layer turbulence within the farm, emphasizing the role of wave-current interaction in creating vertical fluxes and preventing nutrient depletion. Starvation and high Da are most likely to occur in farm blocks with the fully grown profile, caused by increased nutrient consumption due to high kelp density and decreased vertical mixing due to inhibited turbulence in this farm configuration. Additionally, when the spaced kelp rows are oriented perpendicular to the flow direction, the turbulence intensity is demonstrated to be similar to that of farm blocks (Bo et al., 2024). Therefore, nutrient transport in farm blocks is also indicative of farms with rows perpendicular to the flow.

Several strategies for farm development to prevent starvation are proposed. Timely harvest practices can prevent the formation of a fully grown profile, favoring turbulence generation within the farm and ensuring nutrient supply from deeper waters. Densely planted kelp should be avoided, as high frond density can not only increase nutrient consumption, but also lead to flow stagnation in the farm, constraining uptake efficiency and potentially causing kelp starvation. From the perspective of nutrient supply, farms are encouraged to be deployed in regions with relatively strong ocean currents and waves to ensure turbulence generation and nutrient supply. Additionally, selecting a location where the nutricline is relatively shallow, e.g., comparable to the farm base depth, is favorable, so that farm-generated turbulence has the potential to induce the upward nutrient transport.

The Damkohler number Da provides a predictive tool for potential nutrient depletion in the context of farm planning. Accurate calculation of the mixing coefficient is crucial for obtaining a reliable Da. The calculation can be achieved by using hydrodynamic models capable of resolving vertical nutrient transport through the farm. Alternatively, our simulations revealed a positive correlation between the mixing coefficient and turbulence intensity, consistent with the classical mixing length theory. Predicting uptake efficiency based on turbulence intensity thus becomes feasible, which connects to the previous findings on the dependence of turbulence intensity on various farm configurations (Bo et al., 2024).

While we focused on a 400 m farm length, implications of starvation can be extended to longer or infinite farms under similar ocean and nutrient conditions by using Da. In high Da cases, nutrient concentration is expected to decay downstream along the farm, leading to depletion after a distance comparable to the uptake timescale multiplied by mean streamwise velocity. Larger values of Da thus indicate occurrence of depletion over a shorter distance, increasing the risk of starvation. The farms investigated here have an infinite width due to periodic boundary conditions in the y-direction, serving as a suitable proxy for wide farms. We also note that additional standing eddies can be generated on the cross-stream edges of farms with finite width (Tseung et al., 2016), thereby affecting nutrient transport.

This study mainly examines scenarios where the nutricline depth is comparable to the farm base depth. Scenarios where the nutricline is substantially below the farm are not the central focus, as this may inevitably lead to starvation given that farm-generated turbulence would be unable to drive nutrient fluxes from the deep nutricline. In addition, the presence of strong stratification near the ocean surface boundary layer can inhibit vertical mixing (Plew et al., 2006), thus increasing the risk of nutrient depletion (discussed in detail in Supporting Information Text S3). However, strong stratification is seldom a persistent condition in the upper ocean, and a short period of stratification is unlikely to significantly impact farm growth. Moreover, while this study primarily investigates hydrodynamic transport processes affecting nutrient availability, other factors, such as the impact of high temperature on kelp growth, represent additional threats, particularly during El Niño years.

Data Availability Statement

Model data generated in this study are available online at https://doi.org/10.5281/zenodo.10739134.

Acknowledgments

This project was funded by the U.S. Department of Energy ARPA-E MARINER (Macroalgae Research Inspiring Novel Energy Resources) program, grant number DE-AR0000920. The authors acknowledge high-performance computing support from Derecho (doi.org/10.5065/qx9a-pg09) provided by NCAR's Computational and Information Systems Laboratory, sponsored by the National Science Foundation. The authors thank Chao Yan, Daniel Dauhajre, and Daniele Bianchi for helpful discussions.

References

Abdolahpour, M., Ghisalberti, M., Lavery, P., & McMahon, K. (2017). Vertical mixing in coastal

canopies. *Limnology and Oceanography*, *62*(1), 26–42.

Arzeno-Soltero, I. B., Saenz, B. T., Frieder, C. A., Long, M. C., DeAngelo, J., Davis, S. J., & Davis, K. A. (2023). Large global variations in the carbon dioxide removal potential of seaweed farming due to biophysical constraints. *Communications Earth & Environment*, *4*(1), 185.

Bailey, B. N., & Stoll, R. (2013). Turbulence in sparse, organized vegetative canopies: a large-eddy simulation study. *Boundary-Layer Meteorology*, *147*, 369–400.

Bo, T., McWilliams, J. C., Yan, C., & Chamecki, M. (2024). Langmuir turbulence in suspended kelp farms. *under review at Journal of Fluid Mechanics*.

Broch, O. J., & Slagstad, D. (2012). Modelling seasonal growth and composition of the kelp saccharina latissima. *Journal of Applied Phycology*, *24*(4), 759–776.

Cornish-Bowden, A. (2015). One hundred years of Michaelis–Menten kinetics. *Perspectives in Science*, *4*, 3–9.

Craik, A. D., & Leibovich, S. (1976). A rational model for Langmuir circulations. *Journal of Fluid Mechanics*, *73*(3), 401–426.

Dayton, P. K. (1985). Ecology of kelp communities. *Annual Review of Ecology and Systematics*, *16*(1), 215–245.

Deutsch, C., Frenzel, H., McWilliams, J. C., Renault, L., Kessouri, F., Howard, E., … Yang, S. (2021). Biogeochemical variability in the california current system. *Progress in Oceanography*, *196*, 102565.

Ferdouse, F., Holdt, S. L., Smith, R., Murúa, P., & Yang, Z. (2018). The global status of seaweed production, trade and utilization. *Globefish Research Programme*, *124*, 120.

Fernand, F., Israel, A., Skjermo, J., Wichard, T., Timmermans, K. R., & Golberg, A. (2017). Offshore macroalgae biomass for bioenergy production: Environmental aspects, technological achievements and challenges. *Renewable and Sustainable Energy Reviews*, *75*, 35–45.

Finnigan, J. (2000). Turbulence in plant canopies. *Annual Review of Fluid Mechanics*, *32*(1), 519–571.

Frieder, C. A., Yan, C., Chamecki, M., Dauhajre, D., McWilliams, J. C., Infante, J., … others (2022). A macroalgal cultivation modeling system (macmods): evaluating the role of physical-biological coupling on nutrients and farm yield. *Frontiers in Marine Science*, *9*, 752951.

Gerard, V. A. (1982). In situ rates of nitrate uptake by giant kelp, macrocystis pyrifera (l.) c. agardh: tissue differences, environmental effects, and predictions of nitrogen-limited growth. *Journal of Experimental Marine Biology and Ecology*, *62*(3), 211–224.

Ghadiryanfar, M., Rosentrater, K. A., Keyhani, A., & Omid, M. (2016). A review of macroalgae production, with potential applications in biofuels and bioenergy. *Renewable and Sustainable Energy Reviews*, *54*, 473–481.

Haines, K. C., & Wheeler, P. A. (1978). Ammoniun and nitrate uptake by the marine macrophytes hypnea musvuformis (rhodophyta) and macrocystis pyrifera (phaeophyta) 1, 2. *Journal of Phycology*, *14*(3), 319–324.

Huang, I., Rominger, J., & Nepf, H. (2011). The motion of kelp blades and the surface renewal model. *Limnology and Oceanography*, *56*(4), 1453–1462.

Jackson, G. A. (1997). Currents in the high drag environment of a coastal kelp stand off california. *Continental Shelf Research*, *17*(15), 1913–1928.

McWilliams, J. C., Sullivan, P. P., & Moeng, C.-H. (1997). Langmuir turbulence in the ocean. *Journal of Fluid Mechanics*, *334*, 1–30.

Michaelis, L., Menten, M. L., et al. (1913). Die kinetik der invertinwirkung. *Biochemische Zeitschrift*, *49*(333-369), 352.

Monismith, S., Alnajjar, M., Daly, M., Valle-Levinson, A., Juarez, B., Fagundes, M., … Woodson, C. B. (2022). Kelp forest drag coefficients derived from tidal flow data. *Estuaries and Coasts*, *45*(8), 2492–2503.

Nepf, H., Ghisalberti, M., White, B., & Murphy, E. (2007). Retention time and dispersion associated with submerged aquatic canopies. *Water Resources Research*, *43*(4), W04422.

Plew, D. R. (2011). Depth-averaged drag coefficient for modeling flow through suspended canopies. *Journal of Hydraulic Engineering*, *137*(2), 234–247.

Plew, D. R., Spigel, R. H., Stevens, C. L., Nokes, R. I., & Davidson, M. J. (2006). Stratified flow interactions with a suspended canopy. *Environmental Fluid Mechanics*, *6*, 519–539.

Poggi, D., Porporato, A., Ridolfi, L., Albertson, J., & Katul, G. (2004). The effect of vegetation density on canopy sub-layer turbulence. *Boundary-Layer Meteorology*, *111*, 565–587.

Rehage, H., & Kind, M. (2021). The first damköhler number and its importance for characterizing the influence of mixing on competitive chemical reactions. *Chemical Engineering Science*, *229*, 116007.

Renault, L., McWilliams, J. C., Kessouri, F., Jousse, A., Frenzel, H., Chen, R., & Deutsch, C. (2021). Evaluation of high-resolution atmospheric and oceanic simulations of the california current system. *Progress in Oceanography*, *195*, 102564.

Rosman, J. H., Koseff, J. R., Monismith, S. G., & Grover, J. (2007). A field investigation into the effects of a kelp forest (macrocystis pyrifera) on coastal hydrodynamics and transport. *Journal of Geophysical Research: Oceans*, *112*, C02016.

Stevens, C. L., & Hurd, C. L. (1997). Boundary-layers around bladed aquatic macrophytes. *Hydrobiologia*, *346*, 119–128.

Teagle, H., Hawkins, S. J., Moore, P. J., & Smale, D. A. (2017). The role of kelp species as biogenic habitat formers in coastal marine ecosystems. *Journal of Experimental Marine Biology and Ecology*, *492*, 81–98.

Thom, A. (1971). Momentum absorption by vegetation. *Quarterly Journal of the Royal Meteorological Society*, *97*(414), 414–428.

Troell, M., Joyce, A., Chopin, T., Neori, A., Buschmann, A. H., & Fang, J.-G. (2009). Ecological engineering in aquaculture—potential for integrated multi-trophic aquaculture (imta) in marine offshore systems. *Aquaculture*, *297*(1-4), 1–9.

Tseung, H. L., Kikkert, G. A., & Plew, D. (2016). Hydrodynamics of suspended canopies with limited length and width. *Environmental Fluid Mechanics*, *16*, 145–166.

Utter, B. D., & Denny, M. W. (1996). Wave-induced forces on the giant kelp macrocystis pyrifera (agardh): field test of a computational model. *Journal of Experimental Biology*, *199*(12), 2645–2654.

Yan, C., McWilliams, J. C., & Chamecki, M. (2021). Generation of attached Langmuir circulations by a suspended macroalgal farm. *Journal of Fluid Mechanics*, *915*, A76.

Yan, C., McWilliams, J. C., & Chamecki, M. (2022). Overlapping boundary layers in coastal oceans. *Journal of Physical Oceanography*, *52*(4), 627–646.

Zimmerman, R. C., & Kremer, J. N. (1984). Episodic nutrient supply to a kelp forest ecosystem in southern california. *Journal of Marine Research*, *42*(3), 591–604.

Figure 1.

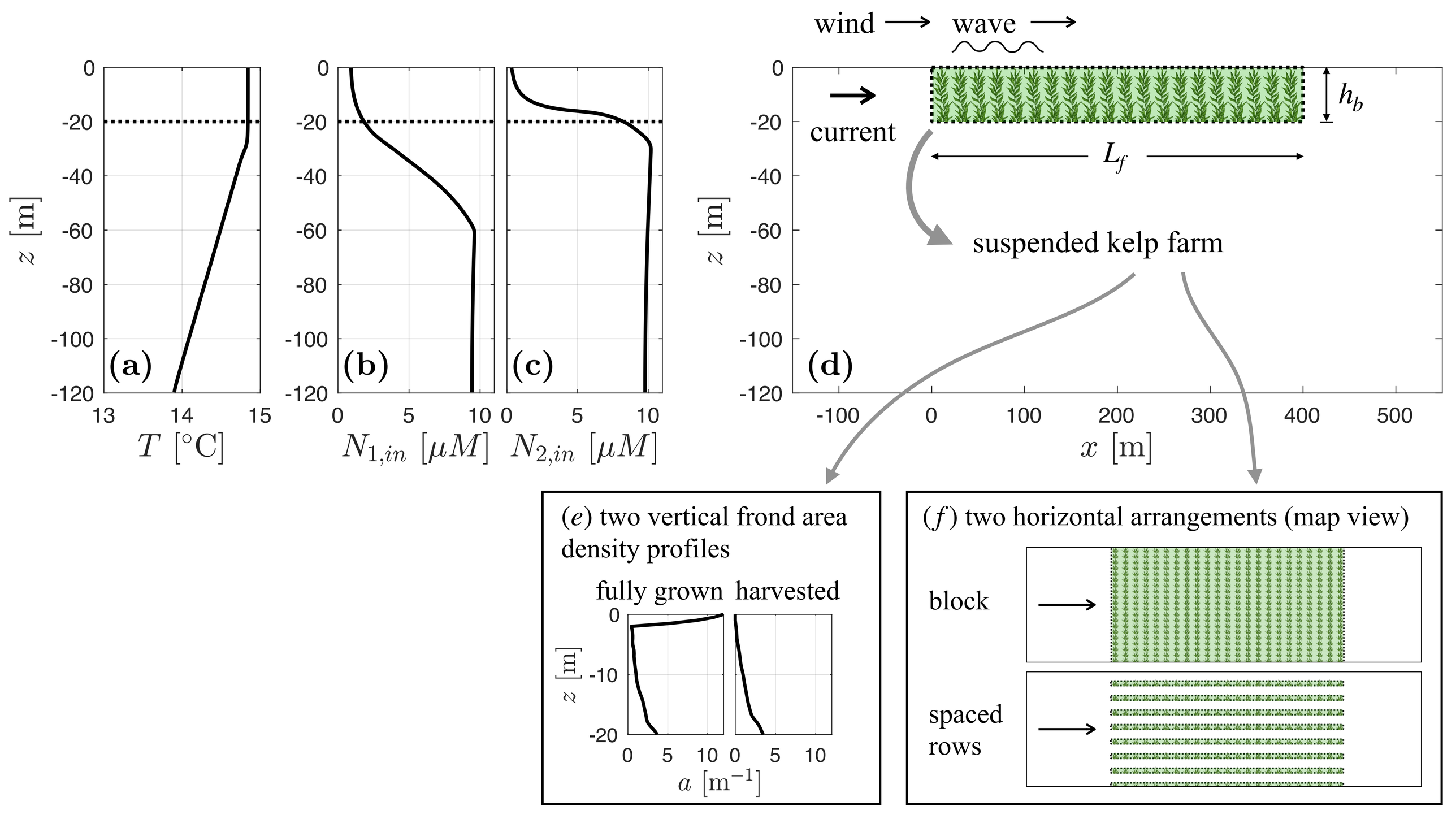
wind
wave
current
h_b
L_f
suspended kelp farm
(a)
(b)
(c)
(d)
z [m]
T [°C]
$N_{1,in}$ [μM]
$N_{2,in}$ [μM]
x [m]
(e) two vertical frond area density profiles
fully grown
harvested
a [m^{-1}]
(f) two horizontal arrangements (map view)
block
spaced rows

Figure 2.

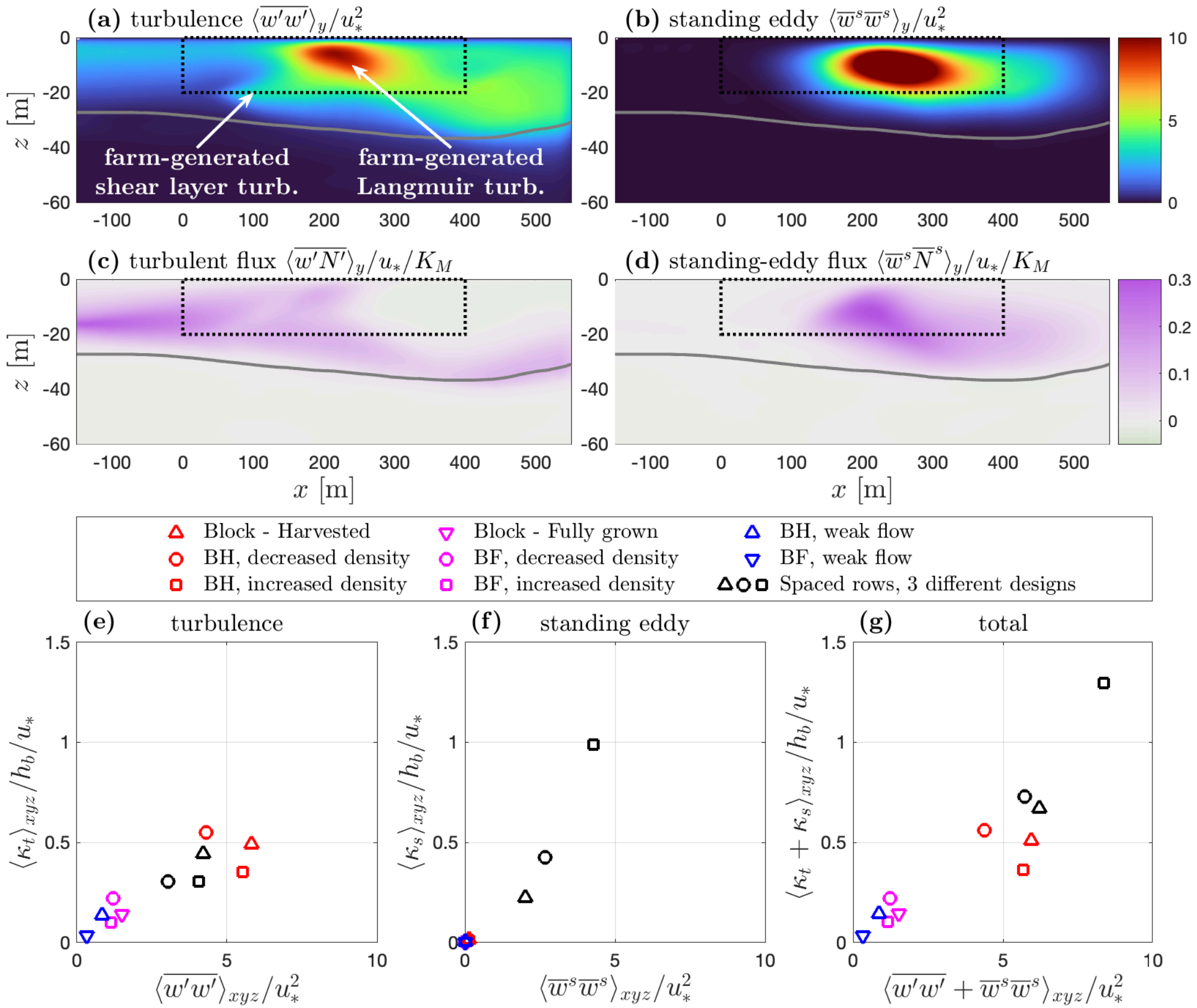
(a) turbulence $\langle \overline{w'w'} \rangle_y / u_*^2$
(b) standing eddy $\langle \overline{w}^s \overline{w}^s \rangle_y / u_*^2$
(c) turbulent flux $\langle \overline{w'N'} \rangle_y / u_* / K_M$
(d) standing-eddy flux $\langle \overline{w}^s \overline{N}^s \rangle_y / u_* / K_M$
farm-generated shear layer turb.
farm-generated Langmuir turb.
z [m]
x [m]
Block - Harvested
BH, decreased density
BH, increased density
Block - Fully grown
BF, decreased density
BF, increased density
BH, weak flow
BF, weak flow
Spaced rows, 3 different designs
(e) turbulence
(f) standing eddy
(g) total
$\langle \kappa_t \rangle_{xyz} / h_b / u_*$
$\langle \kappa_s \rangle_{xyz} / h_b / u_*$
$\langle \kappa_t + \kappa_s \rangle_{xyz} / h_b / u_*$
$\langle \overline{w'w'} \rangle_{xyz} / u_*^2$
$\langle \overline{w}^s \overline{w}^s \rangle_{xyz} / u_*^2$
$\langle \overline{w'w'} + \overline{w}^s \overline{w}^s \rangle_{xyz} / u_*^2$

Figure 3.

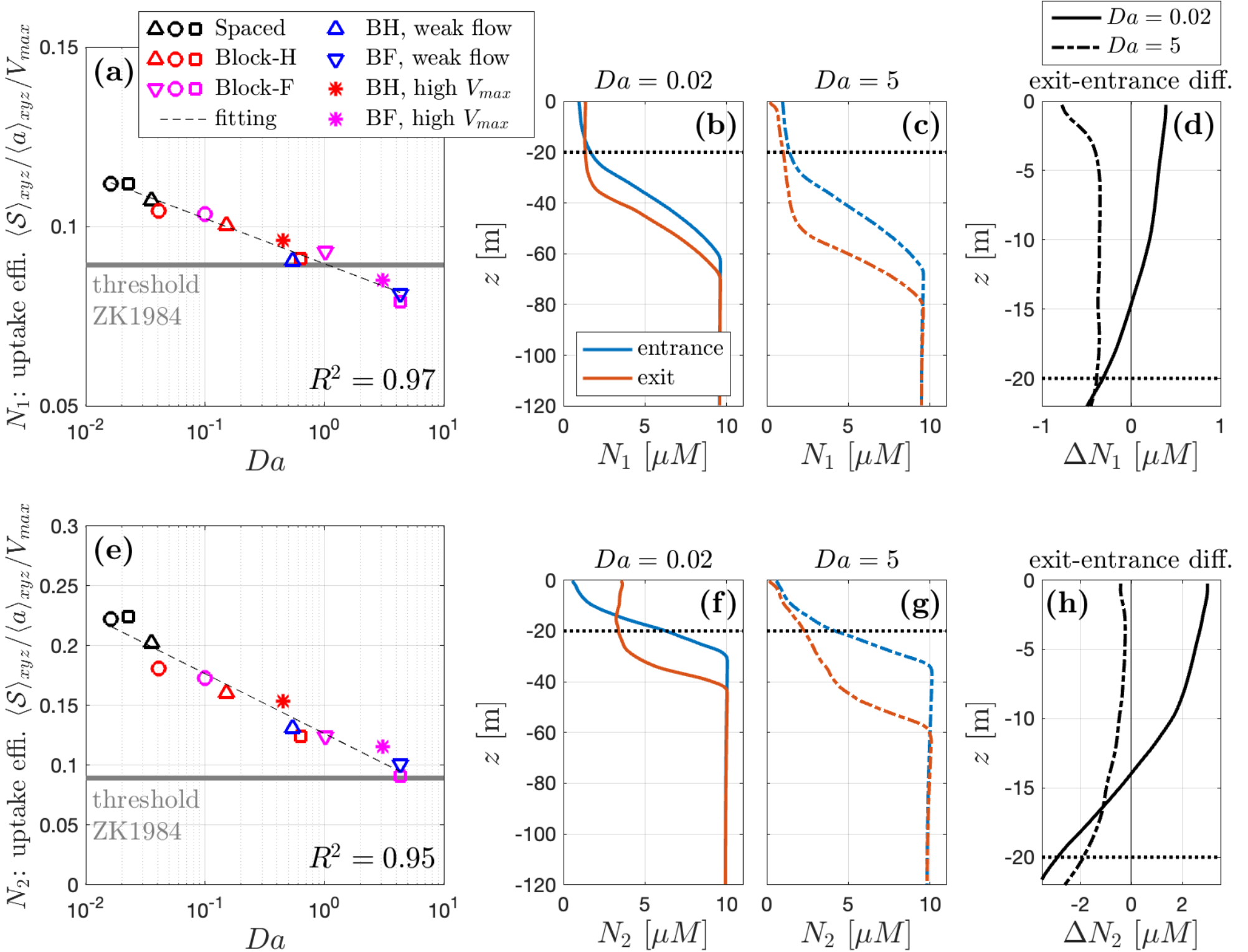
(a)
Spaced
Block-H
Block-F
fitting
BH, weak flow
BF, weak flow
BH, high V_{max}
BF, high V_{max}
threshold
ZK1984
$R^2 = 0.97$
N_1: uptake effi. $\langle \mathcal{S} \rangle_{xyz} / \langle a \rangle_{xyz} / V_{max}$
Da
$Da = 0.02$
$Da = 5$
(b)
(c)
entrance
exit
z [m]
N_1 [μM]
exit-entrance diff.
(d)
ΔN_1 [μM]
(e)
$R^2 = 0.95$
N_2: uptake effi. $\langle \mathcal{S} \rangle_{xyz} / \langle a \rangle_{xyz} / V_{max}$
(f)
(g)
(h)
N_2 [μM]
ΔN_2 [μM]

Figure 4.

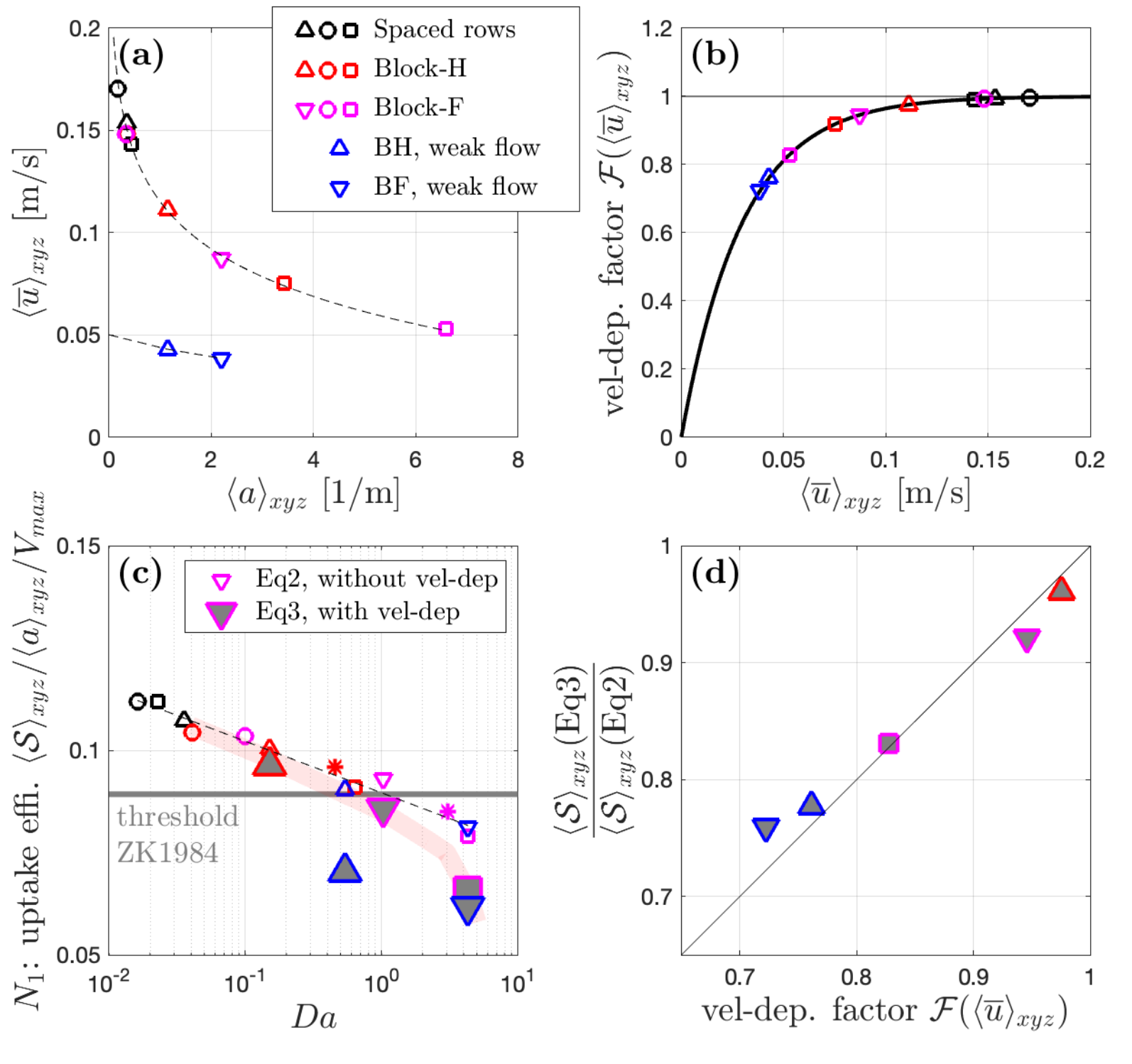
(a)
Spaced rows
Block-H
Block-F
BH, weak flow
BF, weak flow
$\langle \overline{u} \rangle_{xyz}$ [m/s]
$\langle a \rangle_{xyz}$ [1/m]
(b)
vel-dep. factor $\mathcal{F}(\langle \overline{u} \rangle_{xyz})$
$\langle \overline{u} \rangle_{xyz}$ [m/s]
(c)
Eq2, without vel-dep
Eq3, with vel-dep
threshold
ZK1984
N_1: uptake effi. $\langle \mathcal{S} \rangle_{xyz} / \langle a \rangle_{xyz} / V_{max}$
Da
(d)
$\frac{\langle \mathcal{S} \rangle_{xyz}(\mathrm{Eq3})}{\langle \mathcal{S} \rangle_{xyz}(\mathrm{Eq2})}$
vel-dep. factor $\mathcal{F}(\langle \overline{u} \rangle_{xyz})$